IEEE Photonics Journal
An IEEE Photonics Society Publication

Open Access

Beam Transmission Properties in High Power Ytterbium-Doped Tandem-Pumping Fiber Amplifier

Volume 11, Number 2, April 2019

Ping Yan
Zehui Wang
Xuejiao Wang
Qirong Xiao, *Member, IEEE*
Yusheng Huang
Jiading Tian
Dan Li
Mali Gong

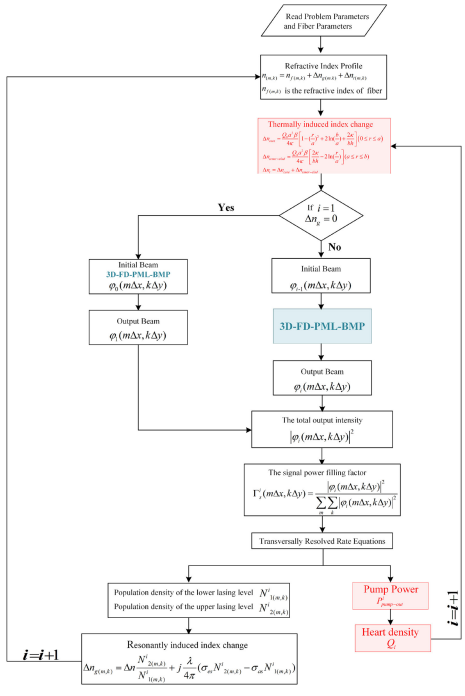

DOI: 10.1109/JPHOT.2019.2906878
1943-0655 © 2019 IEEE

IEEE photonics SOCIETY

IEEE

Beam Transmission Properties in High Power Ytterbium-Doped Tandem-Pumping Fiber Amplifier

Ping Yan,[1,2] Zehui Wang,[1,2] Xuejiao Wang,[1,2,3] Qirong Xiao,[1,2] *Member, IEEE*, Yusheng Huang,[1,2] Jiading Tian,[1,2] Dan Li,[1,2] and Mali Gong[1,2]

[1]Key Laboratory of Photon Measurement and Control Technology, Ministry of Education, Tsinghua University, Beijing 100084, China
[2]State Key Laboratory of Precision Measurement and Instruments, Tsinghua University, Beijing 100084, China
[3]China Academy of Electronics and Information Technology, China Electronic Technology Group Corporation, Beijing 100041, China

DOI:10.1109/JPHOT.2019.2906878

Manuscript received December 11, 2018; accepted March 19, 2019. Date of publication March 25, 2019; date of current version April 11, 2019. This work was supported by the National Natural Science Foundation of China under Grants 61675114 and 61875103, and Tsinghua University Initiative Scientific Research Program under Grant 20151080709. Corresponding author: Qirong Xiao (e-mail: xiaoqirong@mail.tsinghua.edu.cn).

Abstract: This paper presented beam evolution in entire fiber laser from a more qualitative perspective. Specifically, the beam transmission properties under the condition of the disturbances of the refraction index, during the full length of active fiber in tandem pumping fiber amplifier were shown. The refractive index change was calculated considering the laser gain and the thermal effect. The simulations confirmed the superiority on beam transmission when employing the tandem-pumping configuration, which indicated that tandem-pumping fiber lasers might have better control on beam quality than direct-pumping fiber lasers for further power scaling. Moreover, to verify the model, we set a 1080-nm tandem-pumping fiber amplifier with an output power of 5.4 kW and the beam quality M^2 was measured to be 2.2. The experimental result implied a rationality of the model.

Index Terms: Fiber optics amplifiers and oscillators, fiber properties, tandem-pumping.

1. Introduction

With the rapid development of the output power of the ytterbium-doped fiber laser (YDFL) [1], [2] more and more attentions have been paid to tandem-pumping YDFL owing to its attractive characteristics, including stronger pump capacity, lower quantum defect and higher modal instability threshold [3]. Up to now, almost all the achievements realized by tandem pumping YDFLs that set the world record have been held by IPG. In 2009, IPG presented a single mode high power fiber laser (FL) with an output power of 10150 W. The beam quality factor M^2 was measured to be about 1.31 [4]. In 2013, their group increased the output power to 17 kW, along with a beam parameter product of 2 mm mrad because of the 50 μm output fiber core [5]. Apart from IPG, other researchers have also made efforts on tandem pumping FLs. In 2015, Hu Xiao *et al.* presented a 2.14 kW tandem pumping FL in a 30/200 ytterbium-doped fiber (YDF) and the M^2 factor was measured to be 1.9 [6].

In 2017, Pu Zhou *et al.* successfully scaled the output power to the 3.51 kW and the M^2 factor was about 1.98 [3].

With the increasing of power of tandem-pumping FL, there would be some inevitable problems, especially the deterioration of the output beam quality. Effective measures can be taken to improve these conditions if the transmission properties of the beam in the entire gain fiber in the steady state could be acquired. However, there are no reports of the studies on the quantitative theoretical analysis in beam evolution and beam quality of the tandem-pumping fiber amplifier. In fact, this theoretical analysis is challenging for two reasons. First of all, because of small absorption section of Yb icons at 1018 nm, the length of active fiber in tandem-pumping configuration is much longer, typically more than 30 m [3], [6], [7]. Hence, the simulation in the entire active fiber is necessarily computationally intensive and time-consuming without losing the precision. Second, the optical field of the beam is determined by the structure of the waveguide, namely the distribution of refractive index. So the beam evolution can be obtained via the Beam Propagation Method (BPM). However, the gain and thermal effect in the gain fiber could lead to a change of refractive index, which could make an evident impact on the beam evolution. Therefore, besides the BPM, the laser gain and the thermal effect should also be involved to achieve a more reliable analysis.

Cesar Jauregui [8] provided a solid approach for the research of modal interference by combining BPM with transparent boundary conditions (TBCs) and steady state rate equations. However, there study based on direct-pumping configuration and focused a small length of the gain fiber and ignored the thermal effect which should be vital in the case of high power FL. Additionally, TBCs are suitable for single plane wave [9], and can be used in 2D structure [10] or in the simulation that the paraxial approximation is adopted [11], but fail in complicated wave patterns. Considering that the LMA gain fiber in the tandem pump laser is 3D structure and the paraxial approximation is no longer applicable, the TBCs may be not suit. In order to meet those cases, the Perfect Matched Layer (PML) [12], [13] designed to absorb without reflection the electromagnetic waves was applied in this paper. In addition, to reduce the error accumulation in the long distance transmission (more than 30 meters), the second-order wide-angle Padé approximation [14] was employed in the simulation to improve calculation accuracy. Thus, the model we built may be more accurate and more applicable in tandem pump laser.

In this paper, we mainly presented the beam evolution in entire fiber laser from a more qualitative perspective based on tandem-pumping configuration for the first time. The beam transmission properties under the condition of the disturbances of the refraction index, during the full length of active fiber in tandem pumping fiber amplifier were shown. On the one hand, the beam evolution during laser amplification was calculated by 3D-BPM with the boundary condition of PML and second-order wide-angle Padé approximation. On the other hand, the power evolution and the population densities of the upper lasers level were calculated by rate equations. These two methods were connected by the refractive index. Further, the refractive index change was calculated considering the laser gain and the thermal effect. The simulations confirmed the superiority on beam transmission when employing the tandem-pumping configuration, which indicated that tandem-pumping FLs might have better control on beam quality than direct-pumping FLs for further power scaling. Moreover, the results showed that, in any given field of an input beam, the beam transmission properties including the evolution of optical field and the laser intensity, the distribution of fiber temperature and refractive index could be obtained. In order to verify the simulation, a recent result of 5.4 kW tandem pumping fiber amplifier based on master oscillator power-amplifier configuration was presented with a optical-to-optical efficiency of 89.5%, and beam quality M^2 was measured to be 2.2. The trend of the experiment results agreed with that of simulation, implying a rationality of the model.

2. The "B-R" Model

We want to figure out the beam evolution in the fiber amplifier, hence, the BPM method is needed. However, the BPM only describes the beam propagation dynamics in the passive material. Therefore, the BPM with a combination of transversally resolved steady state rate equations will be a

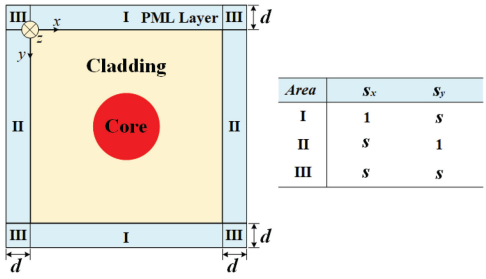

Area	s_x	s_y
I	1	s
II	s	1
III	s	s

Fig. 1. Schematic diagram of the PML.

possible way. Furthermore, the gain and thermal effect in the gain fiber could lead to a change of refractive index, which could make an evident impact on the beam evolution. Hence, we simulated numerically the beam propagation dynamics, the power evolution properties and the thermal effect along the entire gain fiber in the tandem-pumping amplifier. In order to make expression clear, we called our model "B-R" model. Here, "B" and "R" represented BPM and Rate Equations, respectively.

2.1 The BPM Method

The beam evolution dynamics during laser amplifier was simulated by BPM. The basic theory of BPM including notation and general description of the method were followed Ref. [15]. In particular, the PML boundary condition was applied to be a reasonable solution to beam propagation. PML method adopted an absorbing layer in which the matched medium was designed to absorb without reflection the light no matter how large angle the light was. Fig. 1 shows the schematic diagram of the PML, where the Maxwell's equations can be expressed as:

$$\begin{aligned} \nabla' \times \mathbf{H} &= j\omega\varepsilon_0\overline{\varepsilon_r}s\mathbf{E} \\ \nabla' \times \mathbf{E} &= -j\omega\mu_0 s\mathbf{H} \end{aligned} \tag{1}$$

The Eq. (2) can be obtained by Eq. (1) as follows:

$$\begin{aligned} &\nabla' \times \left(\frac{p}{s}\nabla' \times \phi\right) - k_0^2 qs\phi = 0 \\ &\begin{cases} p = 1, q = \overline{\varepsilon_r}, \phi = \mathbf{E} \\ p = \frac{1}{\overline{\varepsilon_r}}, q = 1, \phi = \mathbf{H} \end{cases} \end{aligned} \tag{2}$$

Here ∇' can be represented by Eq. (3) and s can be represented by Eq. (4).

$$\nabla' = \hat{x}s_x\frac{\partial}{\partial x} + \hat{y}s_y\frac{\partial}{\partial y} + \hat{z}s\frac{\partial}{\partial z} \tag{3}$$

$$s = \begin{cases} 1 & outside\ of\ the\ PML \\ 1 - j\frac{(m+1)\lambda}{4\pi dn}\left(\frac{\rho}{d}\right)^m \ln\left(\frac{1}{R}\right) & in\ the\ PML \end{cases} \tag{4}$$

Where λ was the light wavelength, d was the thickness of the PML, ρ represented the surface position of the PML and R stood for the theoretical reflection coefficient. Then the electric field of the signal could be separated into a slowly varying envelope and a fast oscillating phase term in Eq. (2). In order to simplify the solving process and be applicable for wide-angle conditions, the second-order wide-angle Padé approximation was employed in the simulation to get the relationship between $\varphi(z + \Delta z)$ and $\varphi(z)$. It should be point out that 3D scalar approximation was used in the finite-difference (FD) PML BPM method analysis.

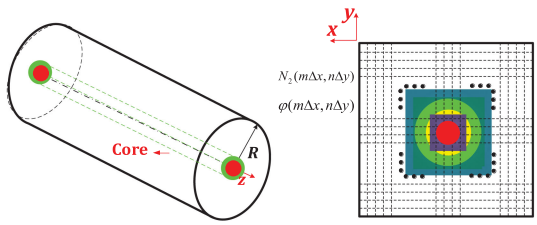

Fig. 2. Schematic diagram of the discretized cross section.

2.2 The Rate Equations

The transversally resolved steady state rate equations were solved by Fourth-Order Runge Kutta (RK) method. In order to be more cooperative with BPM, the rate equations had to be discretized in a rectangular grid, and the corresponding schematic diagram of the discretized cross section was shown in Fig. 2. The solution of each RK iteration was obtained at different z point along the gain fiber, such as the solution at z_0. The refractive index change could be obtained from the solution of iteration. And then this beam could propagate through a section of Δz to a position point of $z_0 + \Delta z$ by using the BPM method basing on the new refractive index distribution. The new beam field could yield the power filling distribution of signal and then a next iteration could be carried out.

2.3 The Change of Refractive Index

Noted worthily, the two methods mentioned above were related by the refractive index. The refractive index change was a key element in our simulation. The refractive index profile was computed by three parts: $n_{(m,k)} = n_{f(m,k)} + \Delta n_{g(m,k)} + \Delta n_{t(m,k)}$. Here, $n_{f(m,k)}$ was the original step refractive index, $\Delta n_{g(m,k)}$ was a result of resonantly induced index change arising from inhomogeneous inversion distribution shown in Eq. 5 [8], [16]. Where, $N_2(m, n)$ and $N(m, n)$ represented the upper levels and the total ion concentration at the transversal point $(m\Delta x, n\Delta y)$, σ_{es} and σ_{as} were the emission and absorption cross-section at the signal wavelength, respectively. Δn was the refractive index change between a fiber region with a fully inversion ($N_2 = N$) and a fiber region with a completely depleted inversion ($N_2 \sim 0$).

$$n_{g(m,n)} = n_g(m\Delta x, n\Delta y) = \Delta n \cdot \frac{N_{2(m,n)}}{N_{(m,n)}} + j\frac{\lambda}{4\pi}\left(\sigma_{es}N_{2(m,n)} - \sigma_{as}N_{(m,n)}\right) \tag{5}$$

$\Delta n_{t(m,k)}$ was thermally induced index change which depended on the pump power distribution and signal laser loss, and the first one had a much higher effect owing to the very small signal loss coefficient [17]–[19]. The temperature in core and cladding of a double cladding fiber were express as:

$$\Delta T_{core} = \frac{Q(z)r_{core}^2}{4\kappa}\left[2\ln\left(\frac{r_{cladding}}{r_{core}}\right) + \frac{2\kappa}{r_{cladding}h}\right] + \frac{Q(z)r_{core}^2}{4\kappa}\left[1 - \left(\frac{r}{r_{core}}\right)^2\right] (0 \le r \le r_{core})$$

$$\Delta T_{cladding} = \frac{Q(z)r_{core}^2}{4\kappa}\left[\frac{2\kappa}{r_{cladding}h} - 2\ln\left(\frac{r}{r_{core}}\right)\right] (r_{core} < r \le r_{cladding}) \tag{6}$$

So that the thermally induced index change in core and cladding of a double cladding fiber could be expressed as:

$$\Delta n_{core} = \frac{Q(z)r_{core}^2\beta}{4\kappa}\left[1 - \left(\frac{r}{r_{core}}\right)^2 + 2\ln\left(\frac{r_{cladding}}{r_{core}}\right) + \frac{2\kappa}{r_{cladding}h}\right] (0 \le r \le r_{core})$$

$$\Delta n_{cladding} = \frac{Q(z)r_{core}^2\beta}{4\kappa}\left[\frac{2\kappa}{r_{cladding}h} - 2\ln\left(\frac{r}{r_{core}}\right)\right] (r_{core} < r \le r_{cladding}) \tag{7}$$

Where, r_{core} and $r_{cladding}$ were the diameter of core and cladding, respectively. $Q(z)$ was the heat density. κ denoted the thermal conductivity. $\beta = dn/dT$ was the thermal-optic coefficient. h was the convection heat transfer coefficient. As a result, the thermally induced index change to the whole double cladding fiber was $\Delta n_t = \Delta n_{core} + \Delta n_{cladding}$.

Above all, the principle diagram of calculation was shown in Fig. 3. By optimizing "B-R" model, a single iteration cycle could only be compressed to a short time. Therefore, our model could be employed to calculate the beam transmission properties in entire gain fiber in next section.

We used this model to simulate the beam transmission of LP01 mode in 20/400 μm. Fig. 4 showed the evolution of the beam intensity along the 1.1 m fiber. Fig. 4(a) descript the transmission of LP01 mode only basing on the BPM methods, and Fig. 4(b) descript the transmission of LP01 mode basing on our new model. Clearly, the interference fringes could be seen from the evolution of the beam transmission in Fig. 4(b). This was because that more modes generated due to the refraction index change, and lead to modes interference inside active fiber.

3. Simulation of the Model

3.1 Comparison of Tandem-Pumping and Direct-Pumping

In our model, the refractive index change showed an evident impact on the beam transmission properties during the whole fiber amplifier. As mentioned above, two factors were included for the causes. One of the factors was laser gain induced by transversal inversion distribution, the other one was thermal effect. It should figure out their impact degree on beam transmission properties.

In order to evaluate their influence, a comparison of the beam transmission properties between the 1018 nm tandem-pumping FL and a 976 nm direct-pumping FL was made. To acquire an adequate absorption, a 18-meter-long 30/400 μm YDF and a 38-meter-long 30/400 μm YDF were employed in the 976 nm direct-pumping FL and 1018 nm tandem-pumping FL, respectively. The absorption coefficients of the YDF were 2.0 dB/m @ 976 nm and 0.45 dB/m @ 1018 nm. In addition, the pump power was both set to be 12000 W.

Fig. 5 plotted the simulation results of the output beam quality under two conditions, where simulation including both factors is marked in '◆' and only the thermal effect is marked in '■' respectively. Clearly, the beam quality remained well when the refractive index change only depended on the thermal effect. Once laser gain was added, the beam quality showed a deterioration, which was especially obvious in Fig. 5(b). It implied that the laser gain made a prominent impact on the beam transmission properties. In addition, the difference of the deterioration degree between the two FLs was owing to their different gain distribution as shown in Fig. 6(a).

Furthermore, it should be noted that the beam quality of 976-nm direct-pumping FL was worse than that of the 1018-nm tandem-pumping FL when considering only the thermal effect. This was because that they differed greatly in temperature distribution inside fiber caused by quantum loss. As shown in Fig. 6(b), the highest temperature at the input end of the 976-nm fiber amplifier was about 276.68 °C while the temperature of the 1018-nm fiber amplifier only 65.06 °C. This analysis above indicated that the thermal effect also had an impact on the beam transmission properties. However, compared with the laser gain, its influence was not as remarkable. Furthermore, the simulation in this section confirmed the superiority on beam transmission of the tandem-pumping FL.

3.2 Simulation of a 5.4-kW Tandem-Pumping Fiber Amplifier

To better understand the beam transmission properties, we did a simulation and did an experiment of a 5.4 kW tandem-pumping fiber amplifier. The parameters used in simulation were shown in Table 1. The structure simulated in "B-R" model was illustrated in Fig. 7(a). The input optical field of the simulation was set to comprise of 70% of LP_{01} mode, 15% $LP_{11\sin\theta}$ mode and 15% of $LP_{11\cos\theta}$ mode for the tandem-pumping amplifier. The corresponding β_{FL} factor [20] of this input field shown

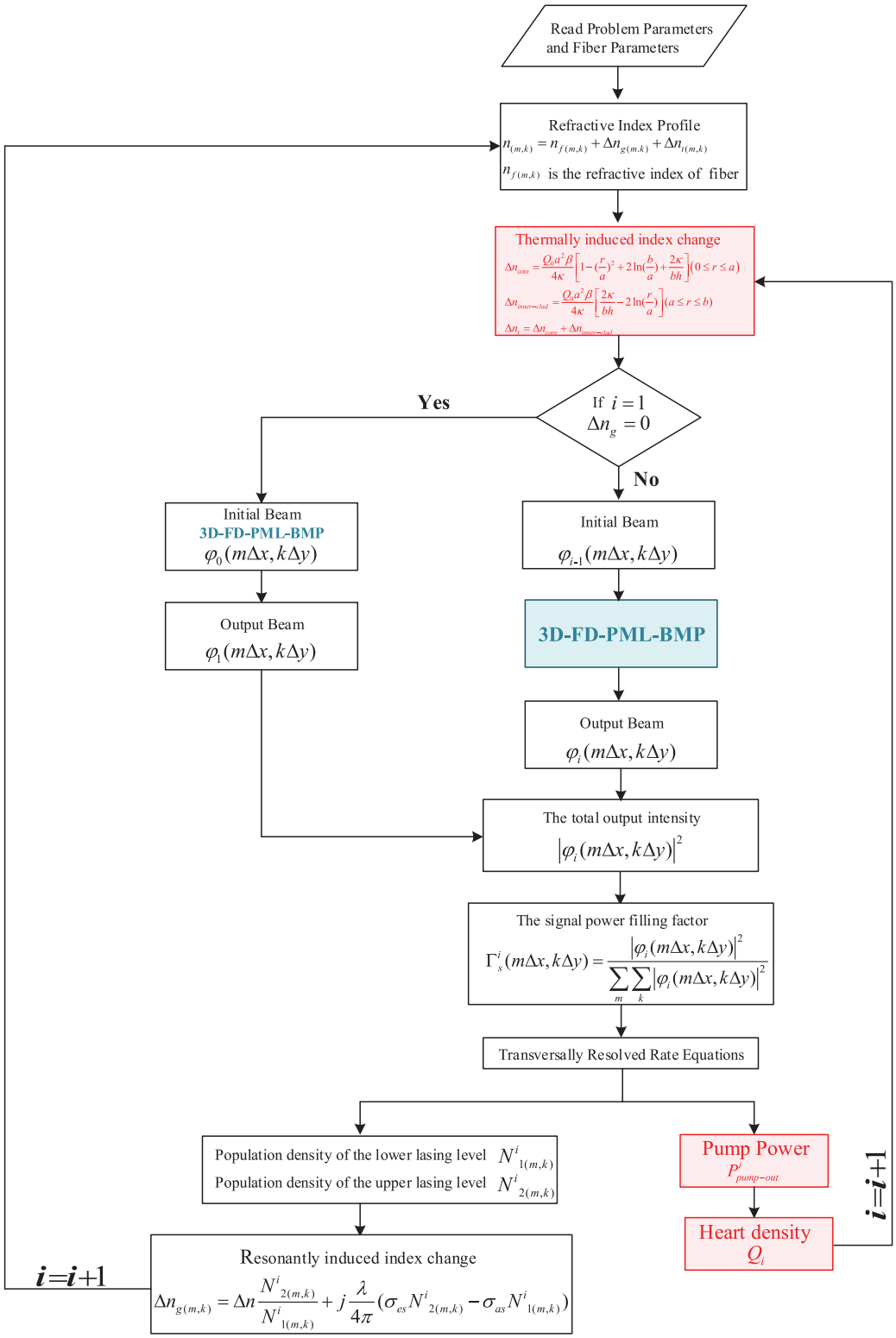

Fig. 3. Principle diagram of calculation.

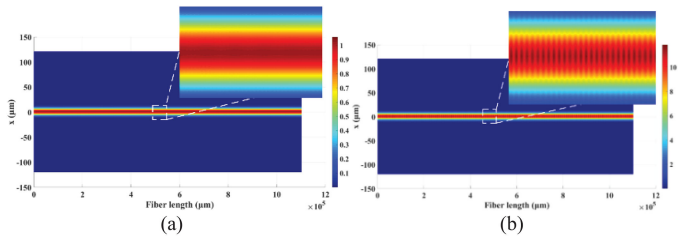

Fig. 4. Evolution of the LP01 beam intensity along the 1.1 m fiber basing on the (a) BPM and (b) "B-R" model.

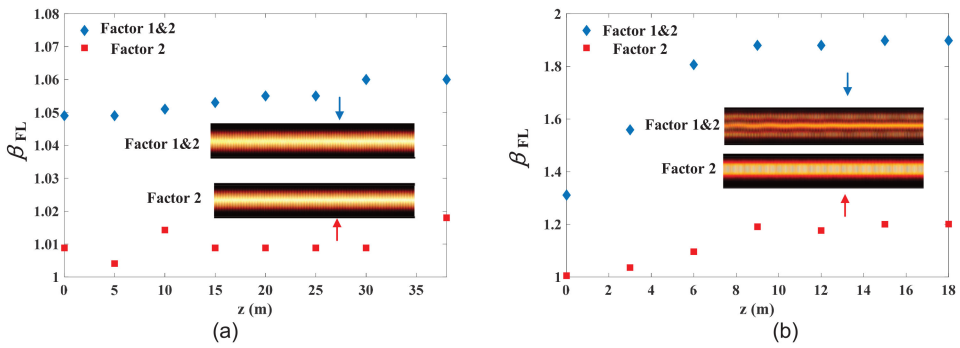

Fig. 5. Results of the output beam quality under two conditions in (a) 1018-nm tandem-pumping FL (the corresponding intensity evolution during 30 m to 38 m was inset) and (b) 976-nm direct-pumping FL (the corresponding intensity evolution during 10 m to 18 m was inset).

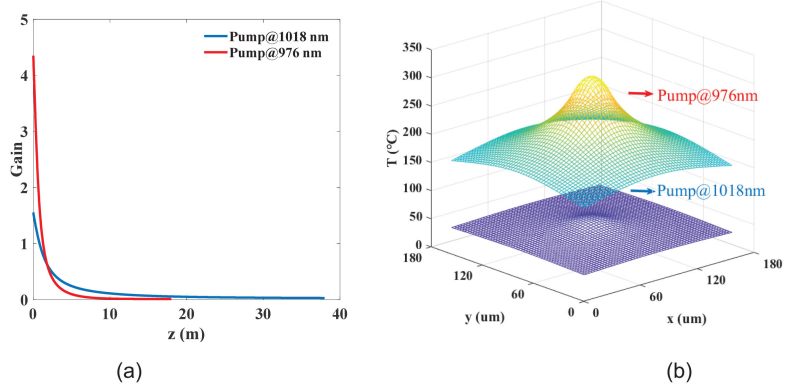

Fig. 6. Differences of (a) the transversal inversion distribution and (b) the temperature distribution at the input end of the amplifier between the 1018-nm tandem-pumping FL and the 976-nm direct-pumping FL.

in the inset of Fig. 7(a) was calculated to be 1.049. Besides, the pump power was set to be 6000 W.

The beam transmission properties calculated by "B-R" model was depicted in Fig. 8(a). Specifically, the z-axis represented the direction of beam transmission and the β_{FL} factor was calculated to characterize the beam quality. The cross-section distributions of the beam at eight different positions in *z* direction were given to indicate the beam evolution along the entire gain fiber. Clearly, the beam quality of the optical field deteriorated gradually along the axis. It was induced by a step change of refractive index caused by the core diameter mismatching of 20 μm and 30 μm in the seed and the amplifier, respectively. Besides, laser gain and thermal effect inside the gain fiber could also lead to disturbances of the refraction index. The change of the refraction index could cause

TABLE 1
The Parameters Used in Simulation

Gain fiber in amplifier	30/250 μm
Numerical aperture	0.06/0.46
Pump power	6000 W
Seed power	75 W
Wavelength of pump light λ_p	1.018 μm
Wavelength of signal light λ_s	1.080 μm
Absorption cross-section of pump light σ_{ap}	7.46×10^{-26} m^2
Emission cross-section of pump light σ_{ep}	5.80×10^{-25} m^2
Absorption cross-section of laser light σ_{as}	2.30×10^{-27} m^2
Emission cross-section of laser light σ_{es}	2.82×10^{-25} m^2
Loss coefficient of pump light α_p	2.0×10^{-3} m^{-1}
Loss coefficient of laser light α_s	2.0×10^{-3} m^{-1}
Refractive index change Δn	1×10^{-5}
Thermal-optic coefficient β	11.8×10^{-6} K^{-1}
Thermal conductivity of silica κ	1.38 W· m^{-1}·K^{-1}
Convection heat transfer coefficient h	4000 W· m^{-2}·K^{-1}
Absorption coefficient of pump light α	0.45 dB· m^{-1}@1018 nm

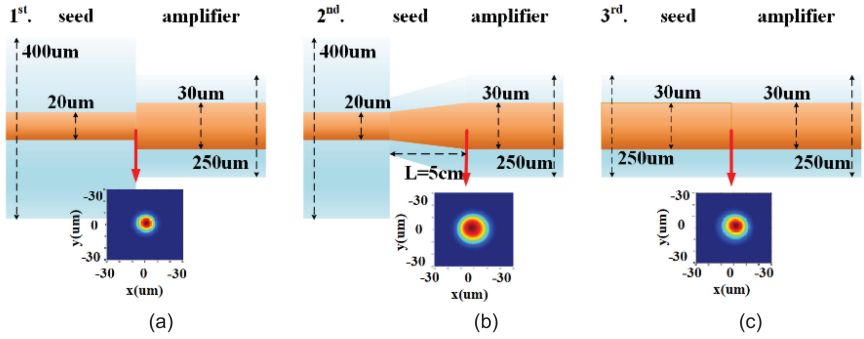

Fig. 7. Three structures of seed lasers and the corresponding input fields for amplifier employing the fiber of 30/250 μm. (a) the different core size fibers are direct spliced with each other. (b) tapered fiber connecting the different size fiber (the core diameter of the narrow end and wide end was 20 μm and 30 μm, respectively.) (c): perfect matching.

the excitation of higher order transverse modes in the 30/250 μm fiber in the amplifier. Fig. 9(a) illustrated the distributions of pump laser and signal laser along the gain fiber. Fig. 9(b) illustrated the ratio of upper level icon concentration to dopant concentration along the gain fiber. The β_{FL} factor at different output power was shown in Fig. 10 (as shown in red line), and when the output power was 5 kW, the β_{FL} factor was calculated to be 1.743.

Furthermore, in order to display the intensity evolution clearly, the intensity distributions during the position from 1 cm to 5 m, 10 m to 15 m, 20 m to 25 m and 30 m to 38 m were shown at the bottom of Fig. 8(a). At the first 5 m, the light intensity was relative weak. However, with the increasing of laser power, the light intensity became stronger and showed a tendency toward stabilization. Fig. 11 shows the cross-section distributions of temperature in *x* and *z* direction. The highest temperature, 43.2 °C, was located at the center of the first cross-section in the gain fiber.

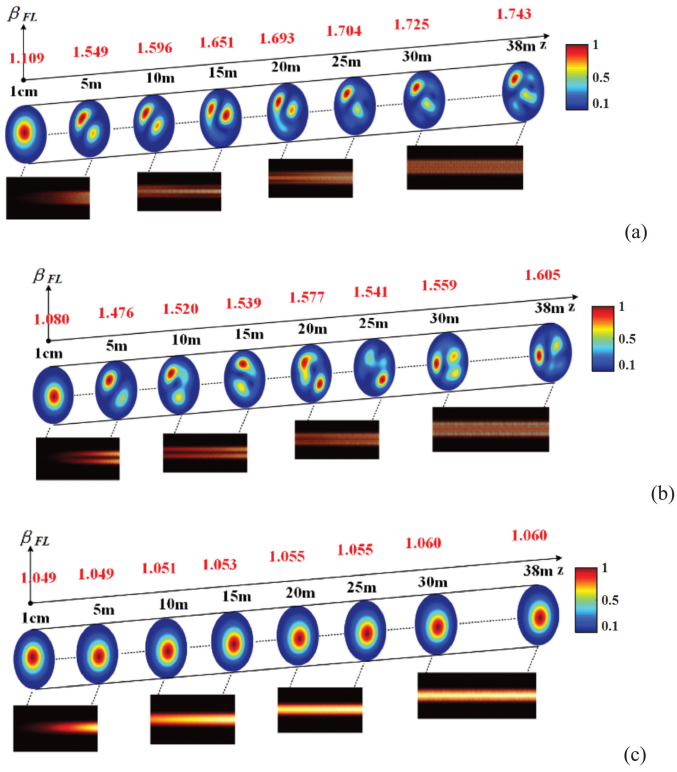

Fig. 8. Beam transmission properties of three structures.

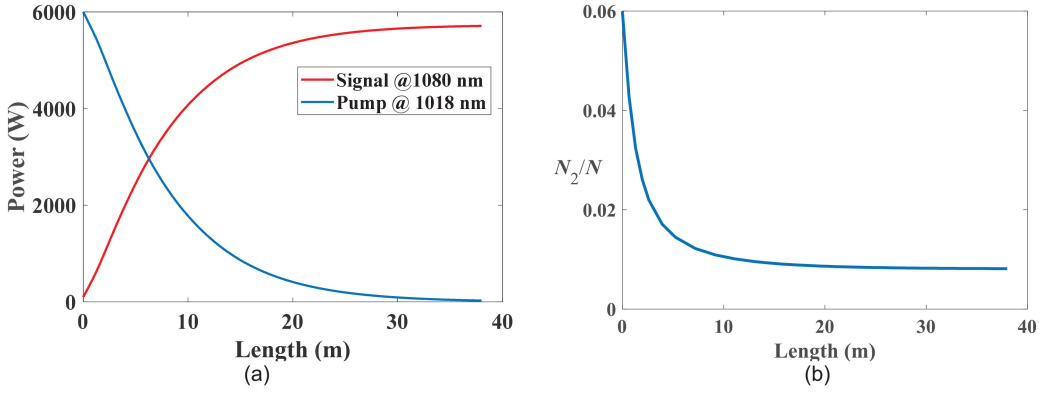

Fig. 9. Distributions of signal and pump laser (a) and ratio of upper level icon concentration to dopant concentration (b) along the gain fiber. N_2: upper level icon concentration, N: dopant concentration.

The temperature gradually decreased along the gain fiber. The distribution of light intensity and temperature indicated in tandem-pumping configuration.

We also simulated the other two structures to analyze the impact of mode matching between the seed and the amplifier. The first structure is a tapered fiber connecting the different size fiber [shown in Fig. 7(b)] and the second structure is perfect matching [as shown in Fig. 7(c)]. In all situations, the pump power was set to be 6000 W. The input optical fields were also kept the same, comprising of 70% LP_{01} mode, 15% $LP_{11\sin\theta}$ mode and 15% $LP_{11\cos\theta}$ mode. In the first case, the change of refractive index was becoming tapered along fiber length. Comparing with the results in Fig. 8(a), the mode excitation reduced owing to a more smooth evolution of the eigenmodes between the fibers of seed and the amplifier. It should be noted that the mode excitation was still exist because the core

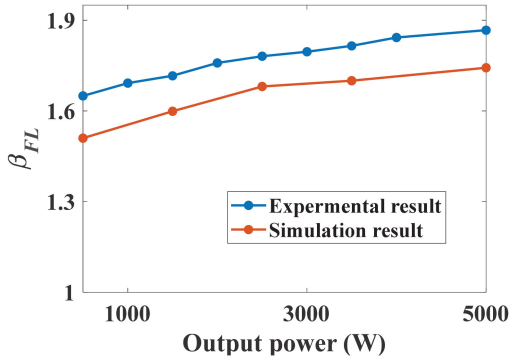

Fig. 10. Beam quality (β_{FL}).of output laser under different output power.

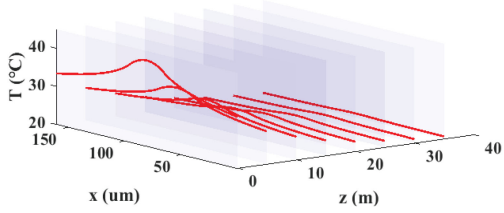

Fig. 11. Temperature distribution along the gain fiber.

size was different in the tapered fiber. Hence, the beam quality during the beam transmission slightly improved, as shown in Fig. 8(b). As for the case of the perfect matching, whose simulation results were illustrated in the Fig. 8(c), the beam distribution remained approximately unchanged during the transmission and the beam quality was the best among all three situations. Therefore, a conclusion could be obtained that the mode matching between the seed and the amplifier in tandem-pumping fiber laser played a significant role in the beam transmission properties. Thus, methods such as improving mode matching and reducing mode-number of the seed could be adopted to obtain a better beam quality in tandem-pumping FL.

4. Verification of the Model

To verify the model, we built a tandem pumping fiber, whose configuration was presented in Fig. 12 [21]. The laser consisted of a 1080 nm laser seed and an amplifier. In the seed, a pair of Bragg gratings (FBGs) formed a resonant cavity whose center wavelength located at 1079.9 nm. A 16-meter-long 20/400 ytterbium-doped fiber was adopted as the gain fiber. The seed emitted a 75 W of output power to the amplifier through the input signal fiber of a homemade $(6 + 1) \times 1$ coupler. The size of coupler's input signal, pump and output fiber were 20/400 μm, 105/125 μm and 30/250 μm, respectively. In amplifier, six 1018 nm homemade fiber lasers [22] were used as the pumping source and were injected into the gain fiber through six pump fibers of the $(6 + 1) \times 1$ coupler. The 1018 nm fiber lasers were pumped by wavelength-stabilized laser diode with high efficiency and high reliability. The total pumping power was about 6000W. The diameters of the core and inner cladding of the gain fiber were 30 μm and 250 μm. The numerical aperture (NA) of gain fiber core and inner cladding were 0.06 and 0.46, respectively. The cladding absorption coefficient was 0.45dB/m @1018 nm. To acquire efficient pump absorption and to suppress the stimulated Raman scattering, the length of the gain fiber was optimized to 38 m. After the gain fiber, a cladding power stripper was spliced to leak the residual pump light. Moreover, a quart block head (QBH) was chosen as the end-cap.

Fig. 13(a) showed the output power in the tandem pumping fiber amplifier. The 75 W seed laser was successfully amplified to 5448 W with a total of 5986 W pump light, corresponding to an

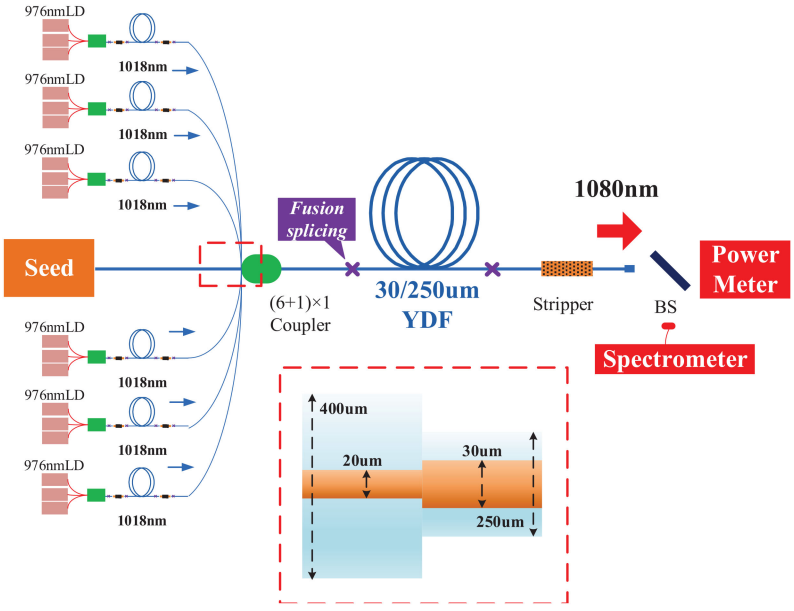

Fig. 12. Experimental setup of tandem-pumping fiber amplifier. Inset: the structure of the seed laser and the amplifier.

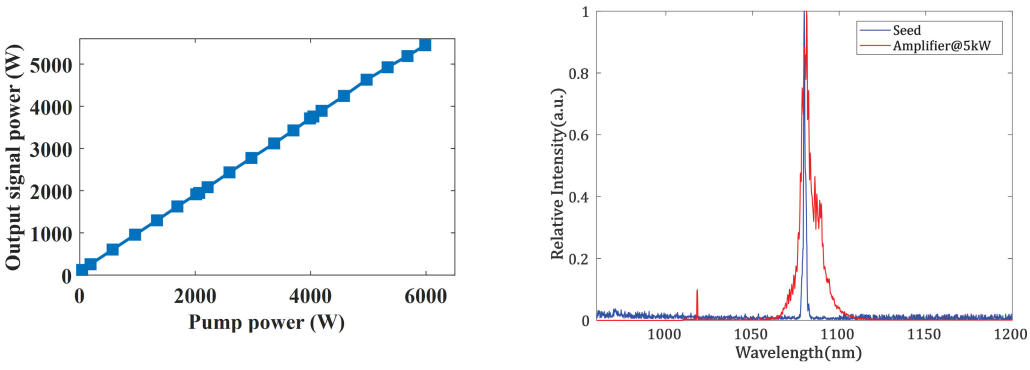

(a) (b)

Fig. 13. Power curve (a) and spectrum (b) of 5.4 kW tandem pumping fiber amplifier.

optical-optical efficiency ($\eta_{o-o} = P_{output}/P_{pump}$) of 89.5%. The 3 dB bandwidth of the spectrum got larger along with the increasing of the pump power, and the 3 dB bandwidth was 4.6 nm at the maximum output power, shown in Fig. 13(b). In addition, no stimulated Raman scattering was found in output spectrum.

The beam quality factor β_{FL} and M^2 of the seed was measured to be 1.12 and 1.27, respectively. After amplifying to 5 kW, the β_{FL} factor was deteriorated to 1.857 and the corresponding M^2 was about 2.2 (indicated by the red line in Fig. 10). The results of the experiment agreed with the simulation ($\beta_{\mathrm{FL}} = 1.743$). The small difference between these two results was mainly caused by core eccentricity in the splicing. Especially, we adopted an end-pumping coupler, in which the splicing of tapered input fiber and output fiber can also cause an inevitable core eccentricity. Even an eccentricity of 1 μm could have an obvious impact on beam quality. In addition, the ideal fiber in the simulation did not exist. Actually, the distributions of refractive index and doping concentration were not uniform along the gain fiber in the experiment, which will also cause a worse beam quality result. For future work, to improve the beam quality of output laser, we plan to use a seed that has the same core size with the amplifier, i.e., the perfect matching structure in Fig. 7(c).

5. Conclusion

In summary, this paper mainly focused on beam evolution in entire fiber laser from a more qualitative perspective for the first time. Specifically, we analyzed the beam transmission properties under the condition of the disturbances of refraction index, during the full length of the active fiber in tandem-pumping fiber amplifier. The refractive index change was calculated by considering both laser gain and the thermal effect. Via our model, the beam transmission properties including the evolution of optical field, the laser intensity, the distribution of fiber temperature and refractive index could be obtained. The simulations also confirmed the superiority on beam transmission when employing tandem-pumping fiber laser. Further, a 1080 nm tandem-pumping fiber amplifier was build. The beam quality M^2 was about 2.2 at full power of 5.4 kW. The experimental result verified the rationality of our model.

References

[1] F. Beier *et al.*, "Single mode 4.3 kW output power from a diode-pumped Yb-doped fiber amplifier," *Opt. Exp.*, vol. 25, pp. 14892–14899, 2017.
[2] Q. Xiao *et al.*, "Bidirectional pumped high power Raman fiber laser," *Opt. Exp.*, vol. 24, pp. 6758–6768, 2016.
[3] P. Zhou *et al.*, "High-power fiber lasers based on tandem pumping," *J. Opt. Soc. Amer. B.*, vol. 34, 2017, Art. no. A29.
[4] V. Gapontsev, V. Fomin, and A. Yusim, "Recent progress in scaling of high power fiber lasers at IPG photonics," in *Proc. Int. Conf. Solid State Diode Laser Technol. Rev.*, 2009, p. 142.
[5] A. Ferin, V. Gapontsev, V. Fomin, A. Abramov, M. Abramov, and D. Mochalov, "17 kW CW laser with 50 μm delivery," in *Proc. 6th Int. Symp. High-Power Fiber Lasers Appl.*, 2012, Session HPFL-1.
[6] H. Xiao, J. Leng, H. Zhang, L. Huang, J. Xu, and P. Zhou, "High-power 1018 nm ytterbium-doped fiber laser and its application in tandem pump," *Appl. Opt.*, vol. 54, pp. 8166–8169, 2015.
[7] Z. H. Wang *et al.*, "3000 W tandem pumped all-fiber laser based on domestic fiber," *Acta Physica Sinica*, vol. 67, no. 2, 2018, Art. no. 024205.
[8] C. Jauregui, T. Eidam, J. Limpert, and A. Tünnermann, "The impact of modal interference on the beam quality of high-power fiber amplifiers," *Opt. Exp.*, vol. 19, pp. 3258–3271, 2011.
[9] G. R. Hadley, "Transparent boundary condition for beam propagation," *IEEE J. Quantum Electron.*, vol. 28, no. 1, pp. 363–370, Jan. 1992.
[10] F. Fogli, G. Bellanca, and P. Bassi, "TBC and PML conditions for 2D and 3D BPM: A comparison," *Opt. Quantum Electron.*, vol. 30, pp. 443–456, 1998.
[11] P. S. Jung, K. Rutkowska, and M. A. Karpierz, "Evanescent field boundary conditions for modelling of light propagation," *J. Comput. Sci.*, vol. 25, pp. 115–121, 2018.
[12] A. Cucinotta, G. Pelosi, S. Selleri, L. Vincetti, and M. Zoboli, "Perfectly matched anisotropic layers for optical waveguide analysis through the finite-element beam-propagation method," *Microw. Opt. Technol. Lett.*, vol. 23, pp. 67–69, 2015.
[13] J. P. Berenger, "A perfect matched layer for the absorption of electromagnetic waves," *J. Comput. Phys.*, vol. 114, pp. 185–200, 1994.
[14] P. Feldmann and R. W. Freund, "Efficient linear circuit analysis by Padé approximation via the Lanczos process," *IEEE Trans. Comput.-Aided Design Integr. Circuits Syst.*, vol. 14, no. 5, pp. 639–649, May 1995.
[15] C. L. Xu and W. P. Huang, "Finite-difference beam propagation method for guide-wave optics," in *Methods for Modeling and Simulation of Guided-Wave Optoelectronic Devices, Part 2: Waves and Interactions (PIERS 11)*, W. P. Huang, Ed. Cambridge, MA: EMW, 1995, pp. 4–13.
[16] M. J. F. Digonnet, R. W. Sadowski, H. J. Shaw, and R. H. Pantell, "Resonantly enhanced nonlinearity in doped fibers for low-power all-optical switching: A review," *Opt. Fiber Technol.*, vol. 3, pp. 44–64, 1997.
[17] Y. Fan *et al.*, "Thermal effects in kilowatt all-fiber MOPA," *Opt. Exp.*, vol. 19, pp. 15162–15167, 2011.
[18] L. Zenteno, "High-power double-clad fiber lasers," *J. Lightw. Technol.*, vol. 11, no. 9, pp. 1435–1446, Sep. 1993.
[19] M. Lapointe, S. Chatigny, M. Piché, M. Cain-Skaff, and J. Maran, "Thermal effects in high-power CW fiber lasers," *Proc. SPIE*, vol. 7195, 2009, Art. no. 71951U.
[20] P. Yan, X. Wang, M. Gong, and Q. Xiao, "Evaluating the beam quality of double-cladding fiber lasers in applications," *Appl. Opt.*, vol. 55, pp. 6145–6150, 2016.
[21] X. Wang *et al.*, "The 5.4 kW output power of the ytterbium-doped tandem-pumping fiber amplifier," in *Proc. Int. Conf. Lasers Electro-Opt.*, 2018, pp. 1–2.
[22] P. Yan *et al.*, "A 1150-W 1018-nm fiber laser bidirectional pumped by wavelength-stabilized laser diodes," *IEEE J. Sel. Topics Quantum Electron.*, vol. 24, no. 3, May/Jun. 2018, Art. no. 0902506.